

THE GAUSSIAN WAVE PACKET TRANSFORM:
EFFICIENT COMPUTATION OF THE SEMI-CLASSICAL LIMIT
OF THE SCHRÖDINGER EQUATION.
PART 1 - FORMULATION AND THE ONE DIMENSIONAL CASE

Giovanni Russo^a and Peter Smereka^b

^aDepartment of Mathematics, University of Catania, Catania, Italy

^bDepartment of Mathematics, University of Michigan, Ann Arbor, Michigan 48109.

Abstract

In this paper an efficient and accurate method for simulating the propagation of a localized solution of the Schrödinger equation near the semiclassical limit is presented. We are interested computing arbitrarily accurate solutions when the non dimensional Plank's constant, ε , is small, but not negligible. The method is based on a time dependent transformation of the independent variables, closely related to Gaussian wave packets. A rescaled wave function, w , satisfies a new Schrödinger equation with a time dependent potential which is a perturbation of the harmonic oscillator, the perturbation being $O(\sqrt{\varepsilon})$, so that all stiffness (in space and time) are removed. In fact, for integration in a fixed time interval, the number of modes required to fully resolve the problem decreases when ε is decreased. The original wave function may be reconstructed by Fourier interpolation, although expectation values of the observables can be computed directly from the function w itself. If the initial condition is a Gaussian wave packet, very few modes are necessary to fully resolve the w variable, so for short time very accurate solutions can be obtained at low computational cost. Initial conditions other than Gaussians wave packets can also be used. In this paper, the Gaussian Wave Packet transform is carefully outlined and applied to the Schrödinger equation in one dimension. Detailed numerical tests show the efficiency and accuracy of the approach. In the sequel of this paper, this approach has been extended to the multidimensional case.

1 Introduction

The semiclassical limit of the Schrödinger equation is a computationally challenging problem that has many applications in chemistry and physics. More specifically, it is concerned with the efficient computation of the initial value problem,

$$\psi_t = \frac{i\varepsilon}{2}\psi_{xx} - \frac{i}{\varepsilon}V(x)\psi \quad \text{with} \quad \psi(x, 0) = A(x) \exp(i\phi(x)/\varepsilon), \quad (1)$$

where $\psi = \psi(x, t) \in \mathbb{C}$, A and ϕ are smooth functions. Here ε denotes the nondimensional Plank's constant, $V(x)$ the potential, and we choose the units so that the mass of the quantum particle is 1.

We are interested in the case $\varepsilon \ll 1$, in this regime the solutions will be highly oscillatory in both space and time on a scale $O(\varepsilon^{-1})$. In many cases, the main interest lies in the numerical computation in several dimensions, for this reason the need to use $O(\varepsilon^{-1})$ modes for each dimension represents a huge computational difficulty.

If ε is not too small, then one can perform a fully resolved calculation both in space and time. A very accurate and efficient method to perform such calculation is based on operator splitting, since the term describing the kinetic energy is very effectively treated in Fourier space, while the term containing the potential can be dealt exactly in real space. For example, a very classic approach is based on Strang splitting (see, for example, [1]), which gives spectral accuracy in $\Delta x/\varepsilon$, and an $O(\Delta t^2/\varepsilon)$ global error in time, as analyzed, for example, in [4]. The step size in space and time are denoted Δx and Δt denote, respectively.

Another very accurate splitting method is the one developed by Chin & Chen [2], which is spectrally accurate in space, and fourth order accurate in time. More precisely, when applied to Eq.(1), the method produces errors which are spectrally small with respect to $\Delta x/\varepsilon$, and of $O(\Delta t^4/\varepsilon)$ in time, as we show in the Appendix. As a consequence, computation of accurate solutions up to a fixed macroscopic time by this method requires a computational effort which is larger than $O(\varepsilon^{-5/4})$ in one space dimension, and larger than $O(\varepsilon^{-d-1/4})$ in dimension d .

If one is interested in the limit of vanishing ε , or at least in the asymptotic limit of very small ε , then there are two powerful approaches for tackling this problem. One of these is based on the WKB approximation in which one looks for solutions of the form $A(x,t)\exp(i\phi(x,t)/\varepsilon)$ and obtains partial differential equations for A and ϕ . At leading order, they describe the behavior in the limit $\varepsilon \rightarrow 0$. The advantage of this approach is that since A and ϕ are smooth functions, the computational cost of this formulation is independent of ε . One difficulty is that ϕ can become multiple valued and A can diverge. This issue can, nevertheless, be overcome (see, for example Refs. [12, 13].)

Another closely related method is based on Gaussian beams or wave packets. A Gaussian wave packet is an exact solution of the Schrödinger equation for a harmonic potential and a very good approximation for an arbitrary potential when $\varepsilon \rightarrow 0$; see, for example, Refs. [6, 9, 11, 14]. The advantage of this approach is that the formulation does not form singularities as the WKB method does. A drawback of the approach is that it is a Lagrangian method and the Gaussian beams may spread out or focus. Recently, Leung & Qian [16] formulated a method based on combining Gaussian beams with an Eulerian approach which inherits the advantages of both.

However, the main disadvantage of the two approaches mentioned above is that *they are only applicable in the limit $\varepsilon \rightarrow 0$* . There is in fact no easy way to improve the accuracy of the solution for a finite ε , at a given time t . Therefore, effects that occur for finite ε are not captured by these formulations. These effects tend to be truly quantum in nature, such as the deviation of expectations from their classical values - see Figure 1. For intermediate regimes, i.e. if ε is small, but not negligible, then fully resolved calculations are expensive (mainly because of the large space resolution needed to resolve small scales), while simple

Gaussian beams are not accurate enough to capture certain quantum effects.

One approach to the small but finite ε case is the work of Faou *et al.* [5], where the authors make use of a set of basis functions computed by Hagedorn [10]. The nice feature of these basis functions is that they include the Gaussian beams as one of their elements, indicating that this method should be well behaved as $\varepsilon \rightarrow 0$. Nevertheless, these authors report a phase error that behaves as $(\Delta t)^2/\varepsilon$. This formalism was extended for scattering problems by Gradinaru *et al.* [8]. Another approach is to consider high order Gaussian beams as was done by Jin *et al.* [15].

Here we propose a different approach to devise an efficient numerical method for the computation of the Schrödinger equation near the semiclassical limit. The strategy is to find a transformation based on Gaussian wave packets that will yield a form of the Schrödinger equation that is much more amenable to numerical computation when $\varepsilon \ll 1$.

The resulting equation is in fact another Schrödinger equation with modified potential (now time dependent). In the limit of vanishing ε the modified potential is harmonic and its ground state corresponds to a Gaussian beam solution of the Schrödinger equation. Furthermore, this modified Schrödinger equation has smooth solutions in the limit as $\varepsilon \rightarrow 0$ indicating it can be accurately approximated with few degrees of freedom.

An important aspect of this work is that the full Schrödinger equation will be computed, and we rely on the connection with Gaussian beams for efficiency, not accuracy. The initial condition for the new equation for the rescaled variable w , for example, does not necessarily represent a Gaussian beam or a finite superposition of Gaussian beams.

The purpose of this paper is to introduce and motivate the Gaussian Wavepacket transform. The exposition is much clearer if the one dimensional case is first considered. Furthermore, to assess the utility of our approach we make comparison with fully resolved simulation of the Schrödinger equation for $\varepsilon \ll 1$. This sort of comparison is more feasible in one dimension. In the sequel to this paper we have shown that the formulation extends to the multidimensional case and, not surprisingly, there are some new features [18]. Nevertheless, our work shows that we can achieve similar results in higher dimensions as well.

Before we present the Gaussian Wavepacket Transform it is useful to first review the method of Gaussian wave packets.

1.1 Gaussian Wave Packets

Heller [11] introduced the approach of solving the semi-classical limit of the Schrödinger equation by representing a solution as sum of Gaussian wave packets. His wave packets took the form:

$$\psi(x, t) = \exp \left[(i/\varepsilon) (\alpha(x - q)^2 + p(x - q) + \gamma) \right] \tag{2}$$

where $\alpha(t)$ and $\gamma(t)$ are complex numbers, while $p(t)$ and $q(t)$ are real, and satisfy the equations of motion of a classical particle. Notice that, separating real and imaginary part of α and γ , the wave function may be written as

$$\psi(x, t) = \exp \left[- \left(\alpha_I(x - q)^2 + \gamma_I \right) / \varepsilon \right] \exp(i\theta/\varepsilon) \quad (3)$$

with $\theta = \alpha_R(x - q)^2 + p(x - q) + \gamma_R$, $\gamma_R(0) = 0$, and $\gamma_I(0)$ chosen so that the initial wave function is normalized, i.e.

$$\int_{-\infty}^{\infty} |\psi(x, 0)|^2 dx = 1.$$

Notice that for $\varepsilon \ll 1$, Eq. (2) represents a highly oscillatory function with a Gaussian envelope centered at $q(t)$. The width of the envelope is proportional to $\sqrt{\varepsilon/\alpha_I}$ where α_I is the imaginary part of α . The wavelength of the oscillations at $x = q$ is $2\pi\varepsilon/p$. The term involving the real part of α gives rise to even finer oscillation in the tails of the wave packet.

In the situation when the potential energy, V , is a quadratic function of x , Heller showed that (2) is an exact solution of (1) provided that

$$\dot{q} = p, \quad (4)$$

$$\dot{p} = -V'(q), \quad (5)$$

$$\dot{\gamma} = \frac{1}{2}p^2 - V(q) + i\alpha\varepsilon, \quad (6)$$

$$\dot{\alpha} = -2\alpha^2 - \frac{1}{2}V''(q). \quad (7)$$

In addition, when the potential is quadratic, it follows that

$$\langle x \rangle = \int_{-\infty}^{\infty} x |\psi(x, t)|^2 dx = q(t),$$

$$\langle p \rangle = \int_{-\infty}^{\infty} \psi^* (-i\varepsilon \partial_x \psi) dx = p(t).$$

There are several important observations to be made about this system. First, the set of o.d.e.s given above is very well behaved as $\varepsilon \rightarrow 0$, and no singularity appears in the Riccati-like equation for α because α is not real. Second, the expected values of both the position and momentum obey the classical equations of motion (4 - 5). Therefore in this setting one can easily compute the semiclassical limit when the initial data takes the form dictated by (2). For general initial conditions one can use a collection of Gaussian wave packets, see, for example, Heller [11] or Leung & Qian [16]. The advantage of this approach is clear, the computational cost is independent of ε , and one needs only to solve four well behaved o.d.e.s for each wave packet. It should also be pointed out that in one dimension Heller's Gaussian

wave packets are the same as Hagedorn's Gaussian beams. This is presumably true in higher dimensions as well.

However, if the potential is not quadratic, then (2) is merely an approximate solution. Indeed, it follows from Theorem 1.1 of [9] (take $\alpha = 1/2$) that if one starts with a Gaussian initial condition then the L^2 error of the Gaussian wave packet is bounded by a quantity that scales like $\sqrt{\varepsilon}$.

Therefore, it is clear that if one needs an accurate solution to the Schrödinger equation one can not depend on just using Gaussian beams since it is not easy to correct the approximation. The goal of this paper is the development of a new formulation of the Schrödinger equation near the semiclassical limit, that takes advantage of the Gaussian beams approximation and that can be more efficiently solved numerically. In this regard, the work of Faou *et al* [5] is quite close in spirit to the aims of this paper. In their work the authors make use of Hagedorn's wave packets to develop an efficient numerical method that is well behaved as $\varepsilon \rightarrow 0$.

Our approach is different and is described in detail in the next section.

2 Wave packets without Gaussians

2.1 Basic Idea

To explain our approach it is useful to first consider a simpler version which begins by transforming Eq. (1) with the following change of variables. Let

$$\psi(x, t) = u(\xi, t) \exp [(i/\varepsilon) (p(t)\xi + \gamma_1(t))], \quad (8)$$

where $\xi = x - q(t)$. The idea then is to choose $q(t)$, $p(t)$, and $\gamma_1(t)$ so that u is less oscillatory in both space and time than ψ . One would then compute u and then invoke (8) to find ψ . If we take a Gaussian wave packet for the initial condition, namely

$$\psi(x, 0) = A \exp [(i/\varepsilon) (\alpha(0)(x - q(0))^2 + p(0)(x - q(0)))]$$

where $A = \exp(-\gamma_I(0))$. Then

$$u(\xi, 0) = A \exp [(i/\varepsilon)\alpha(0)\xi^2].$$

Clearly u is a much smoother function of space than ψ . We now derive an equation for the time evolution of u where we take $\dot{q} = p$, $\dot{p} = -V'(q)$, and $\dot{\gamma}_1 = \frac{1}{2}p^2 - V(q(t))$. One then finds that $u(\xi, t)$ satisfies

$$u_t = \frac{i\varepsilon}{2}u_{\xi\xi} - \frac{i}{\varepsilon}V_1u, \quad (9)$$

where

$$V_1(\xi, t) = V(q(t) + \xi) - V(q) - V'(q(t))\xi$$

Notice the o.d.e.s we find for q, p , and γ_1 are the same as those of the Gaussian wave packet provided we take $\alpha = 0$. There are two reasons why (9) is easier to solve than the usual form of the Schrödinger equation in the semiclassical limit. First, since u is smoother it will require fewer grid points (and Fourier modes) to accurately spatially resolve it. Secondly, it is less stiff. To see this note that

$$V_1(\xi, t) = \frac{1}{2}V''(q(t))\xi^2 + O(\xi^3).$$

Because u is localized in space at $\xi = 0$ it follows that

$$\frac{1}{\varepsilon}V_1u = O(\sigma^2/\varepsilon)$$

where σ is the width of the envelope of ψ . In the usual semiclassical limit one has $\sigma = O(\sqrt{\varepsilon})$ which implies that the second term in (9) is not as stiff as it is in the Schrödinger equation.

2.2 Gaussian wave packet (GWP) transform

The above idea can be further improved by noticing the connection of (8) with the Gaussian wave packet approach. Based on this, it appears natural to consider the following transformation

$$\psi(x, t) = v(\xi, t) \exp \left[(i/\varepsilon) (\alpha(t)\xi^2 + p(t)\xi + \gamma(t)) \right], \quad (10)$$

where $\xi = x - q(t)$. If we let q, p, γ , and α satisfy (4-7), then one finds that

$$v_t = \frac{i\varepsilon}{2}v_{\xi\xi} - 2\alpha\xi v_\xi - \frac{i}{\varepsilon}V_2v, \quad (11)$$

where

$$V_2 = V(q + \xi) - V(q) - V'(q)\xi - \frac{1}{2}V''(q)\xi^2. \quad (12)$$

Notice that if the initial condition is a Gaussian then the initial condition for v is $v(\xi, 0) = A$, which is *very* smooth. Unfortunately the term $2\alpha\xi v_\xi$ makes (11) ill-posed. To see this one notes that in Fourier space $v_t = \frac{1}{2}i\varepsilon v_{\xi\xi} - 2\alpha\xi v_\xi$ transforms to $\hat{v}_t + 2\alpha\partial_k\hat{v} = \frac{1}{2}ik^2\varepsilon\hat{v}$. However, because α is complex, the characteristic speeds have an imaginary component resulting in a ill-posed initial value problem.

To sidestep the issue that (11) is ill-posed we consider a slightly different change of variables namely

$$\psi(x, t) = W(\xi, t) \exp \left[(i/\varepsilon) (\alpha_R(t)\xi^2 + p(t)\xi + \gamma_2(t)) \right], \quad (13)$$

where $\alpha_R(t)$ is now real. If we substitute (13) into (1) while demanding that $\dot{q} = p$ and $\dot{p} = -V'(q)$ one finds

$$W_t + \frac{i\xi^2}{\varepsilon} (\dot{\alpha}_R + 2\alpha_R^2 + V''(q)/2) + \frac{i}{\varepsilon} (\dot{\gamma}_2 - p^2/2 + V(q) - i\alpha_R\varepsilon) W = \frac{i\varepsilon}{2} (W_{\xi\xi} + 4i\alpha_R\xi W_\xi/\varepsilon) - \frac{i}{\varepsilon} V_2 W. \quad (14)$$

If we choose

$$\dot{\gamma}_2 = \frac{1}{2}p^2 - V(q) + i\alpha_R\varepsilon, \quad (15)$$

$$\dot{\alpha}_R = -2\alpha_R^2 - \frac{1}{2}V''(q), \quad (16)$$

then it follows that (13) is a solution of (1) provided

$$W_t = \frac{i\varepsilon}{2} W_{\xi\xi} - 2\alpha_R\xi W_\xi - \frac{i}{\varepsilon} V_2 W, \quad (17)$$

where V_2 is given by (12). At first sight Eq. (17) seems well-posed, unfortunately (16) is a real-valued Riccati equation and can blow up in finite time. To circumvent this difficulty we introduce α_I and demand that $\alpha = \alpha_R + i\alpha_I$ satisfy (7). This means we need to replace (16) by $\dot{\alpha}_R = 2(\alpha_I^2 - \alpha_R^2) - \frac{1}{2}V''(q)$. Clearly (17) must be modified to compensate for this and one finds

$$W_t = \frac{i\varepsilon}{2} W_{\xi\xi} - 2\alpha_R\xi W_\xi - \frac{i}{\varepsilon} F W, \quad (18)$$

where

$$F = V_2 + 2\alpha_I^2\xi^2.$$

Therefore, we have established that (18) with the transformation (13) is a solution of (1) provided:

$$\dot{q} = p, \quad (19)$$

$$\dot{p} = -V'(q), \quad (20)$$

$$\dot{\gamma}_2 = \frac{1}{2}p^2 - V(q) + i\alpha_R\varepsilon, \quad (21)$$

$$\dot{\alpha} = -2\alpha^2 - \frac{1}{2}V''(q). \quad (22)$$

Notice that these equations are almost identical to (4 - 7) with the exception of Eq. (21) where α is replaced by α_R .

Now it is useful to make one last change of variables: we let $w(\eta, \tau) = W(\xi, t)$ where

$$\eta = \xi\sqrt{\alpha_I/\varepsilon} \quad \text{and} \quad \tau = \int_0^t \alpha_I(s) ds. \quad (23)$$

Notice there is no problem with the square root since $\alpha_I > 0$.

With this change of variables (18) becomes

$$w_\tau = \frac{i}{2}w_{\eta\eta} - 2i\eta^2w - \frac{i}{\varepsilon\alpha_I}U(\eta, \tau)w, \quad (24)$$

where

$$U(\eta, \tau) = V\left(q + \eta\sqrt{\varepsilon/\alpha_I}\right) - V(q) - V'(q)\eta\sqrt{\varepsilon/\alpha_I} - \frac{1}{2}V''(q)\eta^2\varepsilon/\alpha_I. \quad (25)$$

The equation for w is a Schrödinger equation for a time dependent potential, in which the explicit dependence on τ is obtained by rewriting system (19–22) using τ as independent variable:

$$\alpha_I \frac{d}{d\tau}q = p, \quad (26)$$

$$\alpha_I \frac{d}{d\tau}p = -V'(q), \quad (27)$$

$$\alpha_I \frac{d}{d\tau}\gamma_2 = \frac{1}{2}p^2 - V(q) + i\alpha_R\varepsilon, \quad (28)$$

$$\alpha_I \frac{d}{d\tau}\alpha = -2\alpha^2 - \frac{1}{2}V''(q), \quad (29)$$

$$\alpha_I \frac{d}{d\tau}t = 1. \quad (30)$$

A Taylor series expansion of U reveals

$$U(\eta, \tau) = \frac{1}{6}V'''(q)\frac{\eta^3\varepsilon^{3/2}}{\alpha_I^{3/2}} + O(\eta^4\varepsilon^2),$$

which implies that

$$w_\tau = \frac{i}{2}w_{\eta\eta} - 2i\eta^2w + O(\sqrt{\varepsilon}). \quad (31)$$

Eq. (18) shows that the error made by the Gaussian beam for a nonharmonic potential is $O(\sqrt{\varepsilon})$. Furthermore, it suggests that if one computes for a time $O(1/\sqrt{\varepsilon})$, then there is no guarantee that the error remains small. In fact, as we shall see, the number of modes needed to have an error less than a given tolerance, δ , scales as $O(t\sqrt{\varepsilon} \log \delta)$.

2.3 Summary of the procedure

Suppose we want to solve the Schrödinger equation with initial data given by a Gaussian wave packet:

$$\psi(x, 0) = \left(\frac{2\beta_I}{\pi\varepsilon}\right)^{1/4} \exp\left[(i/\varepsilon)(\beta(x - x_0)^2 + p_0(x - x_0) + \delta)\right] \quad (32)$$

where $\beta = \beta_R + i\beta_I$ with $\beta_I > 0$. Note that if δ is real then

$$\int_{-\infty}^{\infty} |\psi(x, 0)|^2 dx = 1$$

Then one solves the equation (24) for w with the initial condition

$$w(\eta, 0) = \left(\frac{2\beta_I}{\pi\varepsilon} \right)^{1/4} e^{-\eta^2} \quad (33)$$

and solve the system (26-30) with initial conditions

$$q(0) = x_0, \quad p(0) = p_0, \quad \gamma_2(0) = \delta, \quad \alpha(0) = \beta, \quad \text{and} \quad t(0) = 0.$$

After the function w has been computed in the grid in the η variable, it can be computed on a finer mesh by Fourier interpolation, and the original wave function ψ , satisfying the initial condition (32) can be reconstructed from $w(\eta, t)$:

$$\psi(x, t) = w \left((x - q(t))\sqrt{\alpha_I/\varepsilon}, \int_0^t \alpha_I(s) ds \right) \exp [(-i/\varepsilon)\theta(x, t)] \quad (34)$$

with

$$\theta(x, t) = \alpha_R(t)(x - q(t))^2 + p(t)(x - q(t)) + \gamma_2(t)$$

Notice that observables can be computed directly from w , with no need to reconstruct the original wavefunction. For example the expectation values for position and momentum will be given by Eqs.(35) and (36), as discussed below.

2.4 Deviation from the Classical Trajectory

An interesting consequence of the case of the harmonic potential is that the expectation values of the position and momentum agree with the classical trajectory. The formulation described above allows us to deduce formulas for how much they differ when the potential is not harmonic.

We start with the definitions for the expected values of position and momentum:

$$\langle x \rangle = \int x \psi^* \psi dx \quad \text{and} \quad \langle p \rangle = - \int i\varepsilon \psi^* \partial_x \psi dx,$$

where the $*$ denotes complex conjugate. Using (13) one can show that

$$\langle x \rangle = q(t) + e^{-2Im(\gamma_2)/\varepsilon} \int \xi W^* W d\xi.$$

Figure 1 plots the deviation of $\langle x \rangle$ from $q(t)$ for the situation considered in §3.1. Next, one applies (23) to find

$$\langle x \rangle = q(t) + \frac{\varepsilon}{\alpha_I} e^{-2Im(\gamma_2)/\varepsilon} \int \eta w^* w d\eta. \quad (35)$$

In a similar way one can show

$$\begin{aligned} \langle p \rangle &= p(t) + e^{-2Im(\gamma_2)/\varepsilon} \left(2\alpha_R \int \xi W^* W d\xi - i\varepsilon \int W^* W_\xi d\xi \right), \\ &= p(t) + \varepsilon e^{-2Im(\gamma_2)/\varepsilon} \left(\frac{2\alpha_R}{\alpha_I} \int \eta w^* w d\eta - i \int w^* w_\eta d\eta \right). \end{aligned} \quad (36)$$

2.5 Connection with Gaussian Wave Packets.

In this section we show that if the potential is harmonic and if the initial condition for Eq. (24) is a Gaussian then one recovers (2). Suppose that V is harmonic, then (24) becomes

$$w_\tau = \frac{i}{2} w_{\eta\eta} - 2i\eta^2 w. \quad (37)$$

This means that the GWP transform maps the Schrödinger equation for harmonic potential into another Schrödinger equation for harmonic potential, but with different time and space scale, therefore it is able to completely remove the stiffness, both in space and time.

Suppose now we take for initial data

$$w(\eta, 0) = e^{-\eta^2}.$$

Then one may show that

$$w(\eta, \tau) = e^{-\eta^2 - i\tau}. \quad (38)$$

It then follows from (23) that

$$W(\xi, t) = \exp \left[-\xi^2 \alpha_I(t)/\varepsilon - i \int_0^t \alpha_I(s) ds \right]$$

which implies from (13) that

$$\begin{aligned} \psi(x, t) &= \exp \left[(i/\varepsilon) \left((\alpha_R(t) + i\alpha_I(t))\xi^2 + p(t)\xi + \gamma_2(t) - \varepsilon \int_0^t \alpha_I(s) ds \right) \right] \\ &= \exp \left[(i/\varepsilon) (\alpha(t)\xi^2 + p(t)\xi + \gamma(t)) \right], \end{aligned}$$

the latter equality is given by the observation that $\dot{\gamma} = \dot{\gamma}_2 - \varepsilon\alpha_I$ (compare Eqs. (6) and (21)), which is exactly the Gaussian wave packet given by (2).

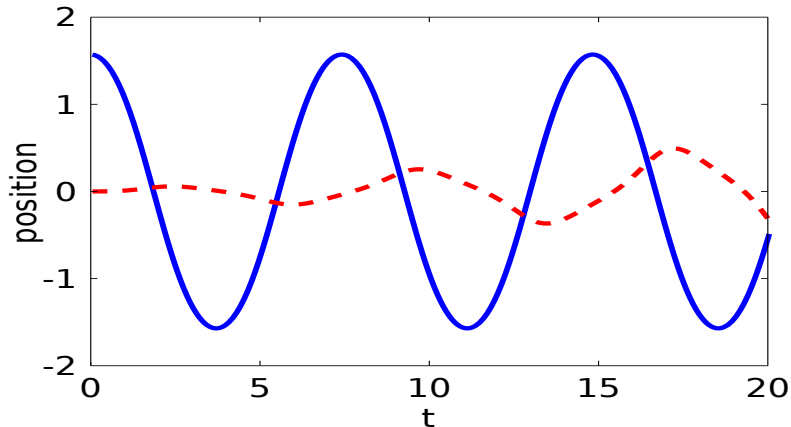


Figure 1: Case 1. The solid blue curve is a plot of $q(t)$ vs. t where as the red dashed curve shows the deviation of expected position from the classical value by plotting $100(\langle x \rangle - q(t))$ vs t

2.6 More general initial data

Our approach easily extends to initial conditions that are not necessarily Gaussian. In particular we can consider initial conditions of the form

$$\psi(x, 0) = f(x - q_0) \exp [(i/\varepsilon)(g(x - q_0) + p_0(x - q_0) + \delta)] \quad (39)$$

where $f(x)$ and $g(x)$ are complex valued smooth functions with $g(0) = g'(0) = 0$ and $\int_{-\infty}^{\infty} |\psi(x, 0)|^2 dx = 1$. In addition, we demand that $Im(g''(0)) \equiv \beta_I > 0$. The initial condition for (24) is then

$$w(\eta, 0) = f(x - q_0) \exp [(i/\varepsilon) (g(x - q_0) - \beta_R(x - q_0)^2)] \quad (40)$$

where $\beta = g''(0)/2$ and $(x - q_0) = \eta\sqrt{\varepsilon/\beta_I}$. The initial conditions for the system (26-30) are

$$q(0) = q_0, \quad p(0) = p_0, \quad \gamma_2(0) = \delta, \quad \alpha(0) = \beta \quad \text{and} \quad t(0) = 0.$$

An example of solution with non Gaussian initial condition is illustrated in Case 3 of Section 3.

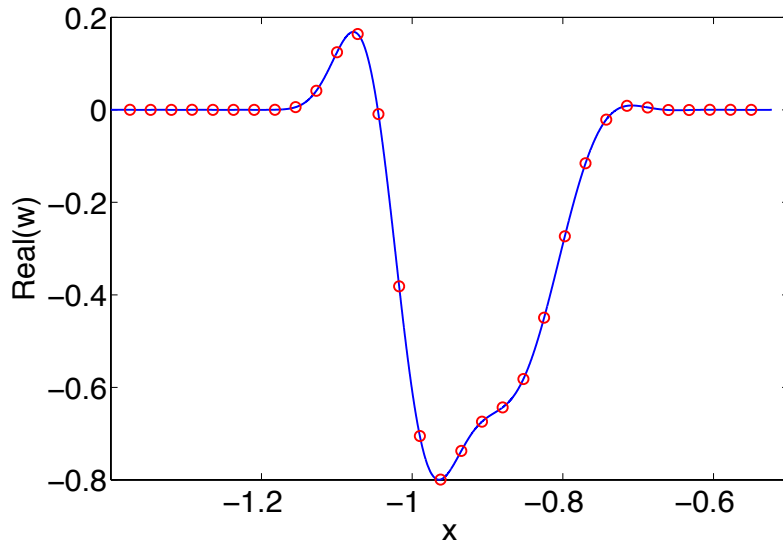


Figure 2: Numerical results for case 1. The real part of w is computed from (24) using $M = 32$, $\Delta\tau = 10^{-2}$, and $\varepsilon = 10^{-3}$ and plotted at $t = 10$. The red circles represent values at the grid points and the blue curve is the Fourier interpolation. The wave function, ψ is constructed from w using (34). This is plotted in Figure 3

2.7 Numerical Implementation

2.7.1 Transformed Schrödinger Equation

The numerical implementation of our approach is fairly straightforward. Here we solve (24) using the method proposed by Chin & Chen [3] (see Eq. (47)) with initial conditions given by (33) in the domain $\eta \in [-\frac{\sigma}{2}, \frac{\sigma}{2}]$ using periodic boundary conditions. Another possible approach is to use Chebychev propagators as proposed by Ndong *et al* [17].

The numerical support of the solution is well inside the computational domain so the use of periodic boundary conditions incurs only a very small error. We will let M denote the number of grid points and let $\Delta\tau$ denote the time step used. The o.d.e. system given by (26-30) is solved using a 4th order Runge-Kutta scheme with a time step $\Delta\tau/40$. We remark that due to the presence of the ε^{-1} terms in the expression given by (34) it is crucial to compute this o.d.e. system with a very small time step to achieve the necessary accuracy.

The above procedure yields a solution for w at the spatial points $\eta_j = j\sigma/M$, where $j = -M/2$ to $M/2 - 1$. As a consequence of (23) then these will correspond to locations in physical space given by $x_j = q(t) + \eta_j \sqrt{\varepsilon/\alpha_I(t)}$. Of course there are too few points to plot the highly oscillatory solution; however, the information is there, it just needs to be

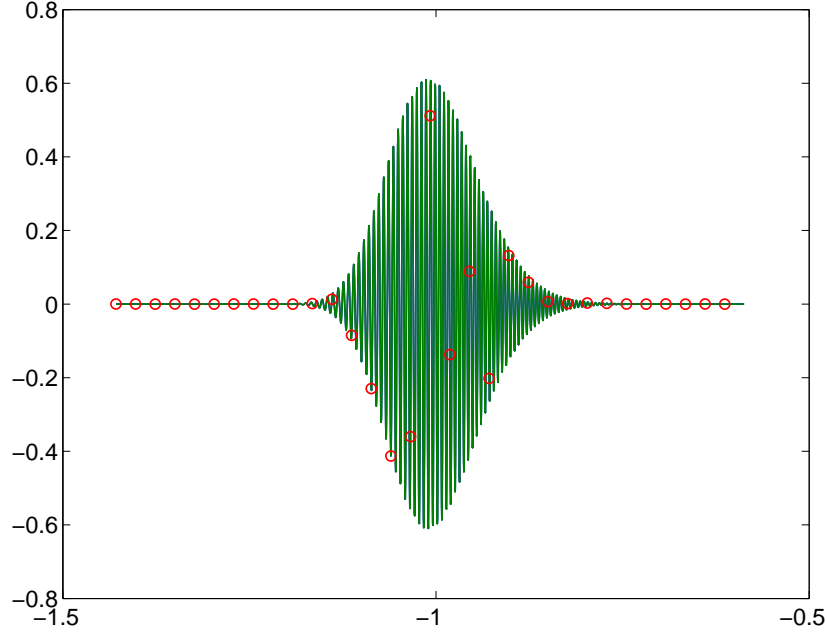


Figure 3: Numerical results for case 1. The real part of the wave function, ψ , is shown at time $t = 10$. It was constructed using w whose real part is plotted in Figure 2. The red circles represent ψ for the 32 grid points in ξ domain. The solution for ψ constructed from the red points using (34) and (41) (Fourier interpolation) is plotted in blue. The green line represents the fully resolved solution computed by fourth order spitting and 2^{16} modes, using a time step 0.001. Due to the excellent agreement with the “exact” solution, the blue line is not visible.

extracted. This task is quite easy to accomplish by Fourier interpolation. To begin we use the Discrete Fourier Transform (DFT) defined as follows

$$\hat{w}_k = \sum_{j=-M/2}^{M/2-1} w_j e^{-i2\pi k\eta_j/\sigma},$$

where w_j are the computed values of w on the grid in the variable η . The inverse of the above formula suggests that we define

$$w_M(\eta) = \frac{1}{M} \sum_{k=-M/2}^{M/2-1} \hat{w}_k e^{i2\pi k\eta/\sigma}. \quad (41)$$

Indeed, $w_M(\eta_j) = w_j$. In this way we can compute values of w for any point η and then use (34) to find values of ψ at any physical location.

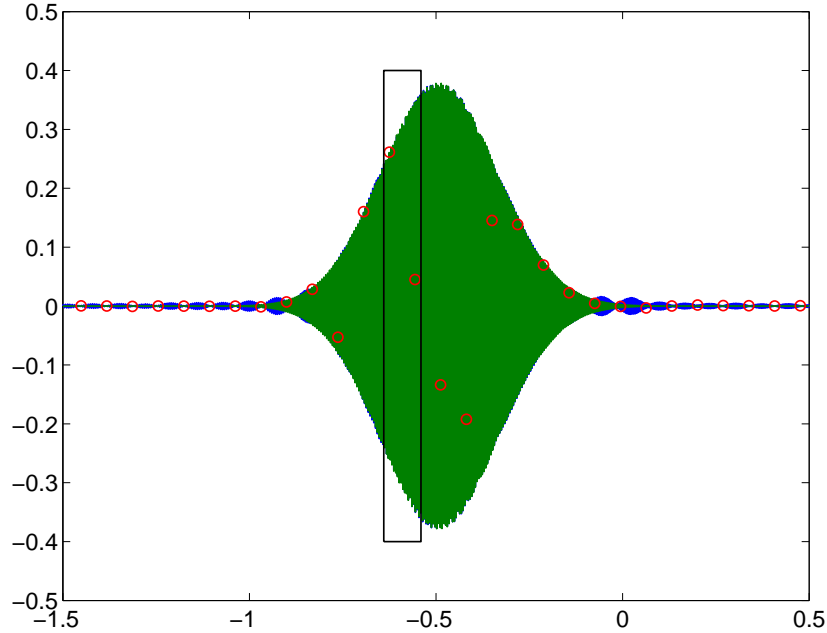


Figure 4: This is same as Fig. 3 except the time is $t = 20$. In this case the error is larger and as a consequence the difference between the “exact” solution from the red points using Fourier interpolation is now visible in the tails of the wave packet. A close-up of the region in the black box is shown in Figure 5

2.7.2 “Exact” Solution

As a benchmark, we will solve the Schrödinger equation directly using the 4th order algorithm given by Eq. (46). The physical domain uses periodic boundary conditions and we let N denote the number of grid points used, which is selected large enough so that the highly oscillatory solution is fully resolved to spectral accuracy. The time step for the reference solution is chosen in such a way to fully resolve the oscillatory behavior. For example, for $\varepsilon = 10^{-3}$, we choose $\Delta t \approx 0.001$. The exact value of Δt is adjusted so that the benchmark solution can be evaluated at the same time as the transformed solution. We shall denote this benchmark solution as the “exact” solution.

2.7.3 Error Evaluation

Our computed solution is compared with the “exact” solution as follows. First we define

$$i_{min} = \lceil x_{min}/\Delta x \rceil \quad \text{and} \quad i_{max} = \lfloor x_{max}/\Delta x \rfloor,$$

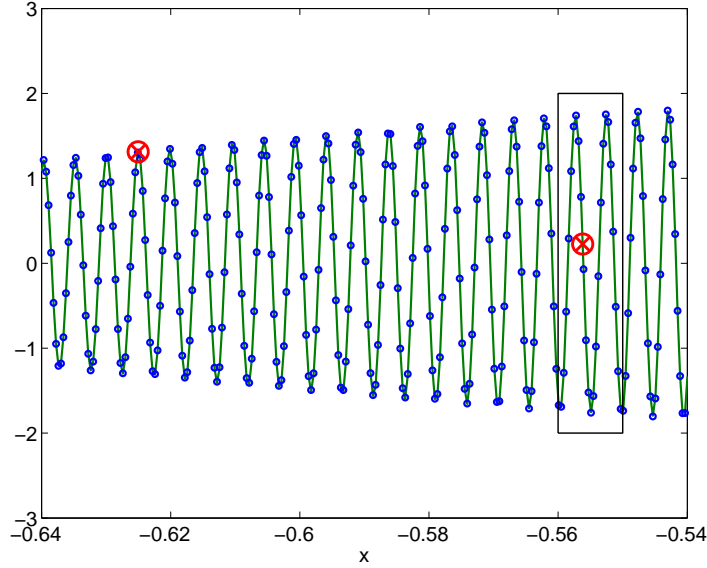


Figure 5: A close up of Fig. 4 except here the computed values (only two are visible) are marked by the large red circles with a cross. The small blue circles represent the solution obtained by Fourier interpolation. The solid green line is the “exact” solution.

where $\Delta x = 2\pi/N$, $x_{min} = q(t) - \frac{1}{2}\sigma\sqrt{\varepsilon/\alpha_I(t)}$, and $x_{max} = q(t) + \frac{1}{2}\sigma\sqrt{\varepsilon/\alpha_I(t)}$ (the interval $[x_{min}, x_{max}]$ is the computation region in physical coordinates; here $\forall x \in \mathbb{R}$, $[x]$ and $\lceil x \rceil$ denote respectively the largest integer smaller than (or equal to) x and the smallest integer larger than (or equal to) x). Then we use Eqs. (34) and (41) to find the computed value of ψ for all grid locations such that $i_{min} \leq i \leq i_{max}$. We shall denote these values as ψ_i^w . The L^2 relative error is then

$$\text{Error}^2 = \frac{\sum_{i=i_{min}}^{i_{max}} |\psi_i - \psi_i^w|^2}{\sum_{i=i_{min}}^{i_{max}} |\psi_i|^2}.$$

In addition, we make comparisons with the Gaussian beam approximation obtained by solving the system (4-7). This was done with a 4th Runge-Kutta scheme with time step $\Delta t_{gb} = \Delta t_n/40$, where $\Delta t_n = t(\tau_n) - t(\tau_{n-1})$.

3 Numerical tests

In all our simulations we consider a domain $x \in [-\pi, \pi]$ with periodic boundary conditions and use the torsional potential

$$V(x) = 1 - \cos x.$$

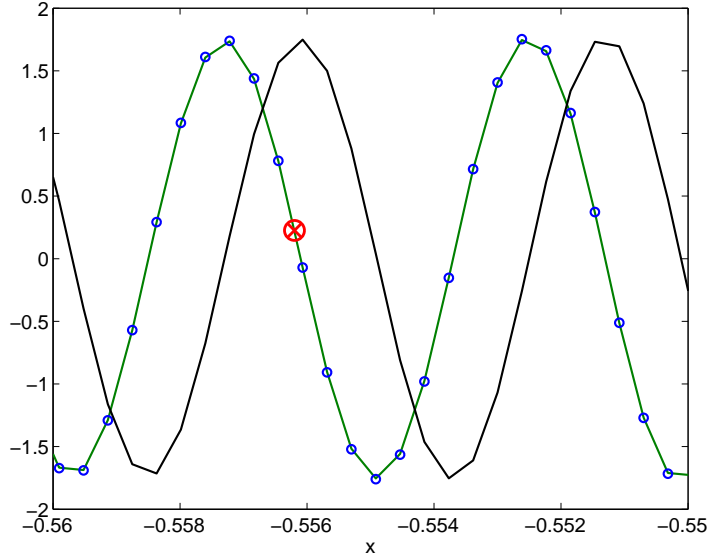


Figure 6: A close up of Fig. 5 except here we have included the Gaussian beam approximation which is plotted with a solid black line. It should be noted that the phase error between the Gaussian beam approximation and the exact solution is $O(1)$.

3.1 Case 1

In the first test case the following initial condition will be used

$$\psi(x, 0) = A \exp \left[(i/\varepsilon) (\alpha_0(x - q_0)^2 + p_0(x - q_0)) \right] \quad (42)$$

where $q_0 = \pi/2$, $p_0 = 0$, $\alpha_0 = 1 + i$, and the normalization constant A is chosen in such that the a way that $\int_{-\pi}^{\pi} |\psi_{(x,0)}|^2 dx = 1$. We will fix $\varepsilon = 10^{-3}$ and examine the behavior of our approach as the number of grid points is varied.

We begin with $M = 32$, $\sigma = 10$ and $\Delta\tau = 0.01$. Figure 1 shows a plot of $q(t)$ vs. t and $\langle x \rangle - q(t)$ as a function of time. This figure shows that the classical trajectory passes through 5 turning points. This plot shows that the deviation between the classical trajectory and the quantum one although small, increases over time. Figures 3-5 show a comparison of the computed solution to the “exact” one. In addition, Figure 6 show a comparison with the Gaussian beam solution which presents a fairly large phase error. Finally, Figure 7 shows a plot of the relative L^2 error as function of time as M and σ are varied. It particular we see that even with very few modes our approach yields solutions that are much more accurate than the Gaussian beam solution.

The exponential increase of the error in time is a direct consequence of two facts: the spectral accuracy of the method in space, and the fact that the number of modes needed to

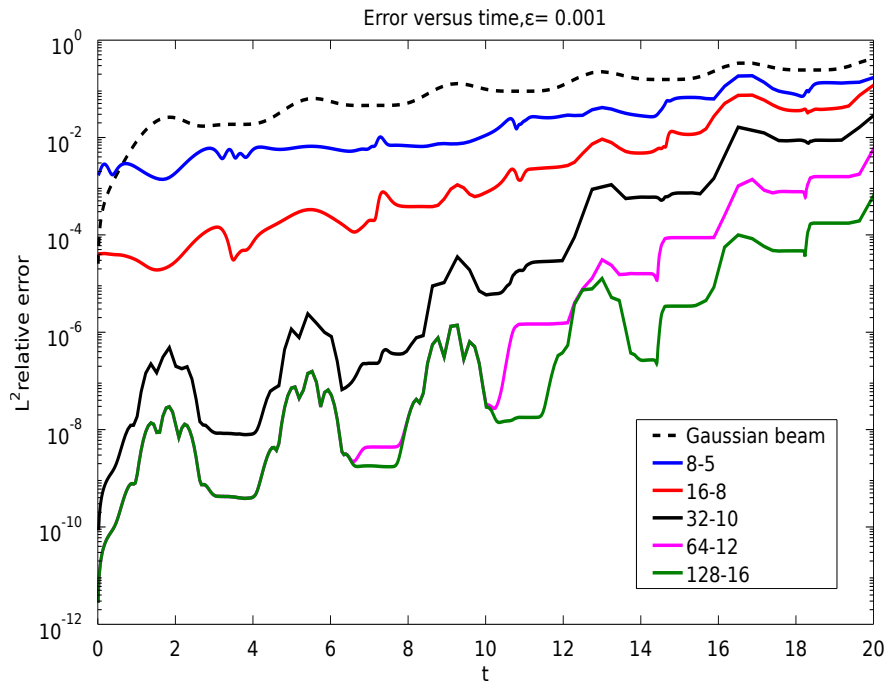


Figure 7: The relative L^2 error is plotted as function of time for the first test problem. Here $\varepsilon = 10^{-3}$, $\Delta\tau = 0.01$. The dashed line represents the error of the Gaussian beam. The two numbers in the legend represent the number of modes used for the w -equation and second number is size of the computational domain, σ . The “exact” solution used $N = 2^{16}$ modes with a time step $\Delta t \approx 0.001$.

fully resolve the function w increases as $t\sqrt{\varepsilon}$.

3.2 Case 2

In this test case we consider how our approach behaves as ε is varied. The same initial condition as in Case 1 are used here. We fix $\Delta\tau = 0.01$, $M = 32$, and $\sigma = 10$. Our “exact” solution uses $N = 2^{14}$ and $\Delta t = 0.001$ for $\varepsilon = 10^{-2}$, $N = 2^{16}$ and $\Delta t = 0.001$ for $\varepsilon = 10^{-3}$, and $N = 2^{18}$ and $\Delta t = 0.001/2$ for $\varepsilon = 10^{-4}$. The relative L^2 errors for the new method and for the Gaussian wave packet are shown in Figure 8. These results show that both methods improve as $\varepsilon \rightarrow 0$. Interestingly, it appears that this new method improves dramatically as $\varepsilon \rightarrow 0$ as compared to the Gaussian wave packet.

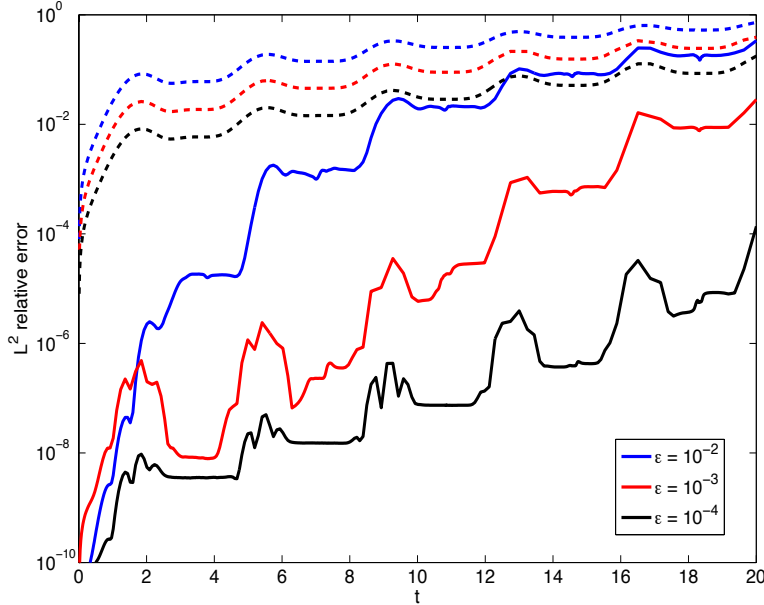


Figure 8: The relative L^2 error is plotted as function of time for three different values of ε . The dashed line represents the error of the Gaussian beam. The new method used $\Delta\tau = 0.01$, $\sigma = 10$, and $M = 32$ for all values of ε .

3.3 Case 3

In this part, we check the method by using initial conditions which are not a Gaussian packet. We consider two initial conditions, the first is

$$\psi(x, 0) = A(x - x_0) \exp(-(x - x_0)^2/\varepsilon) \exp(i \cos(x - x_0)/\varepsilon) \quad (43)$$

where $x_0 = \pi/2$ and A is chosen so that $\int_{-\pi}^{\pi} |\psi(x, 0)|^2 dx = 1$. The results are plotted in Figure 9 and the error evolution is plotted in Figure 10.

The second choice is given by

$$\psi(x, 0) = A f(x - x_0) \exp(-h(x - x_0)/\varepsilon) \exp(i \cos(x - x_0)/\varepsilon) \quad (44)$$

where $f(x) = x + x^2$ and $h(x) = x^2 + \frac{1}{2}x^4$. The error evolution is plotted in Figure 10.

In both cases we see that the error evolution is comparable to the cases where the initial condition was a Gaussian even though these two choices are quite different from a Gaussian.

Recall that for a harmonic potential our method is essentially exact for Gaussian initial data, because it corresponds to numerically solving the Schrödinger equation for harmonic

potential with smooth initial data, Eq. (37). This property manifests itself even for non Gaussian initial data. Indeed, if we consider (43) as initial data for the Schrödinger equation with a harmonic potential, then one finds that error remains very small (observe the red line in Figure 10).

4 Conclusions

In this paper, we have proposed an efficient approach for solving the Schrödinger equation in the semiclassical regime. This formulation is based on a transformation, inspired by Gaussian wave packets, that maps the Schrödinger equation into another Schrödinger equation which is much more amenable to solution in the semi-classical limit and offers a significant improvement over Gaussian wave packets. Indeed with just 32 modes this approach is orders of magnitude more accurate than the Gaussian wave packet approximation. Furthermore, we have provided evidence that this method is robust as $\varepsilon \rightarrow 0$; in fact as expected it inherits the property from Gaussian beams which is that the method becomes more accurate as $\varepsilon \rightarrow 0$. We have also explored the possibility of initial conditions which are not Gaussians; the results presented here indicate that this approach can be applied to a wide class of initial conditions. We have shown in the sequel to this paper that the ideas behind the Gaussian wavepacket transform extend naturally to higher dimensions as well. Extensions of the method, including adaptive time stepping and adaptive meshing in space are currently under investigation.

Appendix: Splitting methods

We begin our discussion by first writing (1) in the form

$$\psi_t = (A + B)\psi, \tag{45}$$

where $A = (i\varepsilon/2)\partial_{xx}^2$ and $B = -iV/\varepsilon$.

2nd order splitting

Second order Strang splitting is given by

$$\psi^{n+1} = e^{\frac{1}{2}\Delta t B} e^{\Delta t A} e^{\frac{1}{2}\Delta t B} \psi^n.$$

The $e^{\Delta t A}$ term can be computed efficiently with spectral accuracy using a fast Fourier transform (FFT) and the number of modes needed scales as $O(\varepsilon^{-1})$. The temporal discretization error comes from the fact that operators A and B do not commute. One can verify that

$$S_2 \equiv \left[e^{\Delta t(A+B)} - e^{\frac{1}{2}\Delta t B} e^{\Delta t A} e^{\frac{1}{2}\Delta t B} \right] \psi = O(\Delta t^3/\varepsilon),$$

where the expression for S_2 is given below. The above formula indicates that the local truncation error is $O(\Delta t^3/\varepsilon)$, meaning that method is formally second order accurate. In addition, it suggests that one needs to take a time step $o(\sqrt{\varepsilon})$ to achieve good accuracy as $\varepsilon \rightarrow 0$. See, for example, [4].

4th order splitting

There are many 4th order splitting methods and they all require that at least one stage takes a backward time step. In fact Suzuki [19] proved a theorem showing that this is necessary. One popular choice is the method due to Forest & Ruth [7]. In the application of this method to the Schrödinger equation, Chin & Chen [2] showed that such a scheme is not much better than second order Strang splitting because the 4th order splitting error has a large pre-factor. They then demonstrate that another class of 4th order splitting methods greatly out performs the one due to Forest & Ruth. One of the 4th order schemes studied by Chin & Chen [2] is

$$\psi^{n+1} = e^{\frac{1}{6}\Delta t B} e^{\frac{1}{2}\Delta t A} e^{\frac{2}{3}\Delta t C} e^{\frac{1}{2}\Delta t A} e^{\frac{1}{6}\Delta t B} \psi^n \quad (46)$$

where

$$C = \frac{-i}{\varepsilon} \left(V(x) - \frac{\Delta t^2}{48} (V'(x))^2 \right)$$

The strength of this 4th order scheme is that no negative time step is required. We note that the introduction of the operator, C , means Suzuki's theorem [19] concerning negative time steps does not apply. One can show that the splitting error is

$$S_4 \equiv \left[e^{\Delta t(A+B)} - e^{\frac{1}{6}\Delta t B} e^{\frac{1}{2}\Delta t A} e^{\frac{2}{3}\Delta t C} e^{\frac{1}{2}\Delta t A} e^{\frac{1}{6}\Delta t B} \right] \psi = O((\Delta t)^5/\varepsilon)$$

where the expression for S_4 is given below. The above formula indicates that the local truncation error is $O((\Delta t)^5/\varepsilon)$. This means that the method is formally 4th order accurate and that one needs to take a time step $o(\varepsilon^{1/4})$ to achieve good accuracy as $\varepsilon \rightarrow 0$.

Chin and Chen [3] also show how to extend (46) to the case of time dependent potentials. The result is

$$\psi^{n+1} = e^{\frac{1}{6}\Delta t B(t_{n+1})} e^{\frac{1}{2}\Delta t A} e^{\frac{2}{3}\Delta t C(t_n+\Delta t/2)} e^{\frac{1}{2}\Delta t A} e^{\frac{1}{6}\Delta t B(t_n)} \psi^n. \quad (47)$$

Expressions for the Splitting Error

Here we give the formulas for the splitting error for both the second order and fourth order schemes. Both of these expressions we computed using MathematicaTM.

The leading order term in splitting error for 2nd order Strang splitting is

$$S_2 = \frac{-i(\Delta t)^3}{48\varepsilon} \left[(V'(x))^2 \psi + \varepsilon^2 (4V''(x)\psi_{xx} + 4V'''(x)\psi_x + V''''(x)\psi) \right]$$

It follows from the work of Descombes and Thalhammer [4] that the local truncation error is in fact $O(\Delta t^3/\varepsilon)$, and therefore the above expression is exact apart from terms $o(\Delta t^3/\varepsilon)$.

In addition they proved that for a class of high order splitting schemes of order p , the local truncation error is $O(\Delta t^{p+1}/\varepsilon)$. The method of Chin and Chen does not belong to the class of splitting schemes considered in [4], and therefore their theory does not apply here.

The leading order error (in time) for the 4th order splitting method is

$$S_4 = \frac{i(\Delta t)^5}{138240\varepsilon} [P_0 + \varepsilon^2 P_2 + \varepsilon^4 P_4]$$

where

$$\begin{aligned} P_0 &= 64(V')^2 V'' \psi \\ P_2 &= 96(V'')^2 \psi_{xx} + 288V'V''' \psi_{xx} + 480V''V''' \psi_x + 136(V''')^2 \psi \\ &\quad + 288V'V^{(4)} \psi_x + 192V''V^{(4)} \psi + 72V'V^{(5)} \psi \\ P_4 &= 48V^{(4)} \psi_{xxx} + 96V^{(5)} \psi_{xxx} + 72V^{(6)} \psi_{xx} + 24V^{(7)} \psi_x + 3V^{(8)} \psi \end{aligned} \quad (48)$$

We conjecture that the above formula is exact up to $O(\Delta t^6/\varepsilon)$ terms, and it would be interesting to further analyze the error, in order to prove or disprove such a conjecture.

Acknowledgments

G. Russo and P. Smereka were supported in part by the National Science Foundation through Grants DMS-0810113 and DMS-1115252, and the *Laboratory for Complex Systems* of the *Scuola Superiore di Catania*.

References

- [1] W. Bao, S. Jin, P.A. Markowich, On time-splitting spectral approximations for the Schrödinger equation in the semiclassical regime, *J. Comput. Phys.* **175** 487-524 (2002).
- [2] S.A. Chin and C.R. Chen, Fourth order gradient symplectic integrator methods for solving the time-dependent Schrödinger equation, *J. Chem. Phys.* **114** 7338-7341, (2001).
- [3] S.A. Chin and C.R. Chen, Gradient symplectic algorithms for solving the Schrödinger equation with time dependent potentials *J. Chem. Phys.* **117** 1409-1415, (2002).

- [4] S. Descombes and M. Thalhammer, An exact local error representation of exponential operator splitting methods for evolutionary problems and applications to linear Schrödinger equations in the semi-classical regime, *BIT Numerical Mathematics* **50** 729-749 (2010).
- [5] E. Faou, V. Gradinaru, and C. Lubich, Computing semiclassical quantum dynamics with Hagedorn wavepackets, *SIAM J. Sci. Comput.* **31**, 3027-3041 (2009).
- [6] E. Faou and C. Lubich, A Poisson integrator for Gaussian wavepacket dynamics, *Comput. Vis. Sci.* **9**, 45-55 (2006).
- [7] E. Forest and R.D. Ruth, Fourth-order symplectic integration, *Physica D* **43**, 105-117 (1990).
- [8] V. Gradinaru, G.A. Hagedorn, and A. Joyce, Tunneling dynamics and spawning with adaptive semiclassical wave packets, *J. Chem. Phys.* **132** 184108 (2010).
- [9] G.A. Hagedorn, Semiclassical quantum mechanics. I. The $\hbar \rightarrow 0$ limit for coherent states, *Commun. Math. Phys.* **71**, 77-93 (1980).
- [10] G.A. Hagedorn, Raising and lowering operators for semi-classical packets, *Ann. Physics* **269** 77-104 (1998).
- [11] E.J. Heller, Time dependent approach to semiclassical dynamics, *J. Chem. Phys.* **62**, 1544-1555 (1974).
- [12] S. Jin and X. Li, Multi-phase computations of the semiclassical limit of the Schrödinger equation and related problems: Whitham vs Wigner, *Physica D* **182**, 46-85 (2003).
- [13] S. Jin and S. Osher, A level set method for the computation of multivalued solutions to quasi-linear hyperbolic PDEs and Hamilton-Jacobi equations, *Comm. Math. Sci.* **1**, 575-591 (2003).
- [14] S. Jin, H. Wu, and X. Yang, Gaussian beam methods for the Schrödinger equation in the semi-classical regime: Lagrangian and Eulerian formulations, *Commun. Math. Sci.* **6** 995-1020 (2008).
- [15] S. Jin, H. Wu, and X. Yang, Semi-Eulerian and high order gaussian beam methods for the Schrödinger equation in the semiclassical regime, *Commun. Comput. Phys.* **9** 668-687 (2011).
- [16] S. Leung and J. Qian, Eulerian Gaussian beams for Schrödinger equations in the semi-classical regime, *J. Comput. Phys.* **228**, 2951-2977 (2009).

- [17] M. Ndong, H. Tal-Ezer, R. Kosloff, and C.P. Koch, A Chebychev propagator with iterative time ordering for explicitly time-dependent Hamiltonians, *J. Chem. Phys.* **132** 064105 (2010).
- [18] G. Russo and P. Smereka, The Gaussian Wave Packet Transform: Efficient Computation of the Semi-Classical Limit of the Schrödinger Equation. Part 2 - The Multidimensional Case, in preparation.
- [19] M. Suzuki, General theory of fractal path integrals with applications to many-body theories and statistical physics, *J. Math. Phys.* **32** 400-407 (1991).

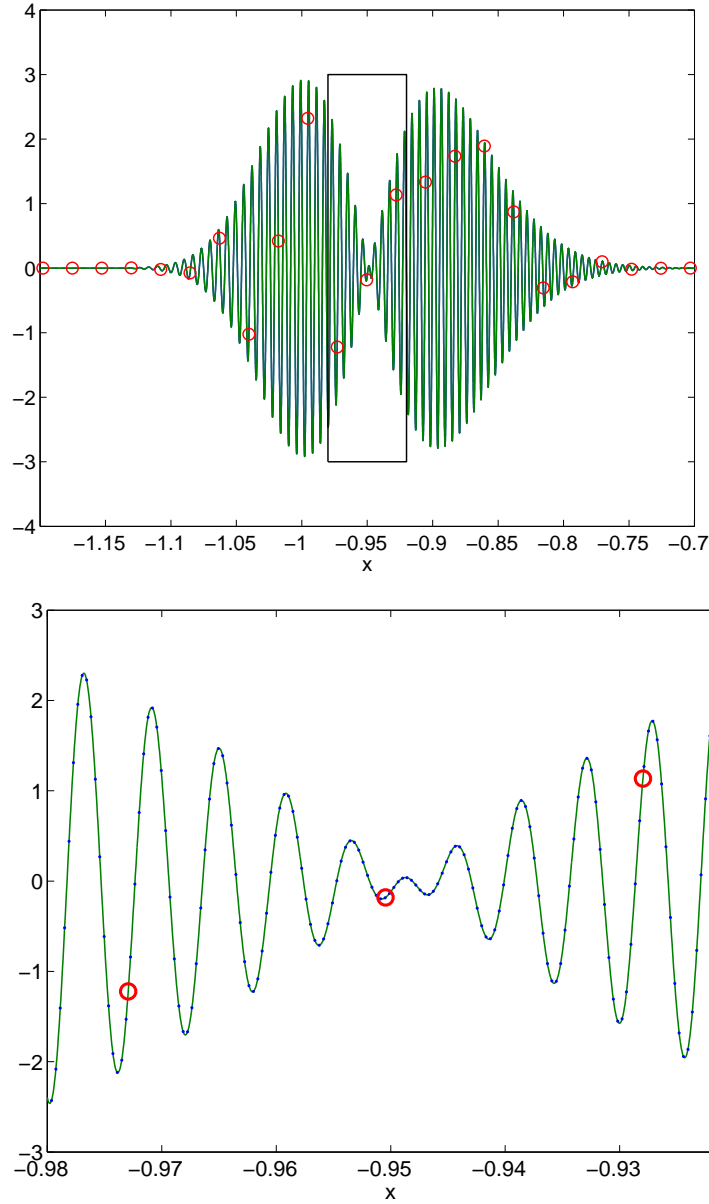


Figure 9: Real part of the wave function at time $T = 10$ for the non-Gaussian initial condition given by (43). The green line represents the fully resolved calculation. In the upper figure, the numerical solution is reconstructed and printed in blue line, which is not visible, because it is covered by the green line. In the zoom (lower picture) the blue dots represent the computed solution reconstructed on a fine grid, while the red circle represent the computed solution on the original $M = 32$ point grid. $\varepsilon = 10^{-3}$ and $\sigma = 10$.

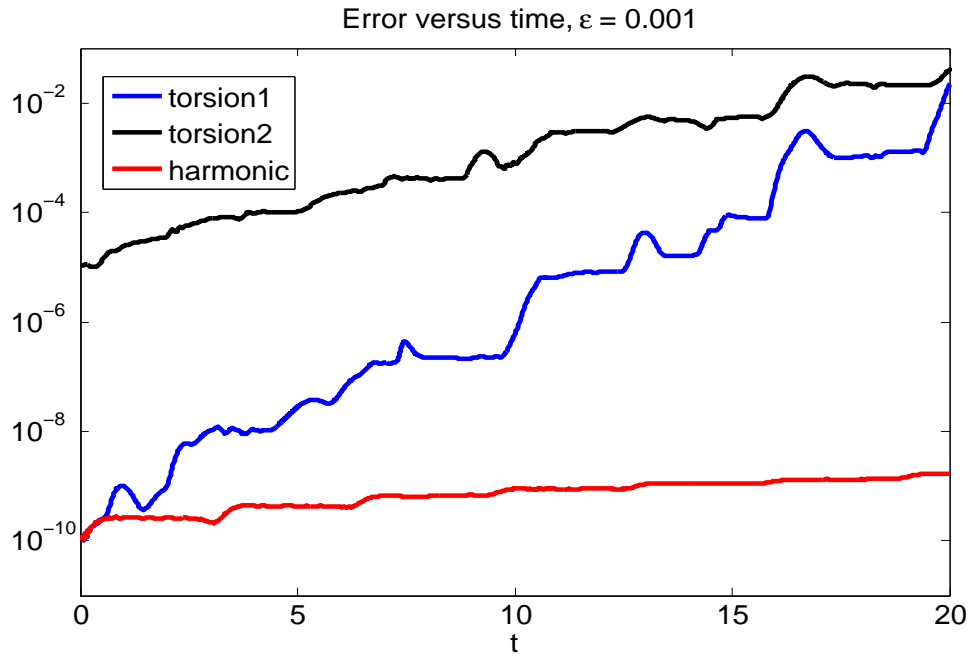


Figure 10: Relative error as a function of time for non Gaussian initial condition (Case 3). The blue and black curves correspond to the initial condition given by Eq. (43) (solved with $M = 32$ and $\sigma = 10$), and Eq. (44) (solved with $M = 64$ and $\sigma = 14$), respectively, using the torsional potential. The red curve corresponds to the case using the initial condition given by (43) ($M = 32$, $\sigma = 10$), using a harmonic potential. In the latter case, the error remains small after a large time, and there is no need to approximate the initial condition as a superposition of Gaussian beams.